

Rapid optimal work extraction from a quantum-dot information engine

Kushagra Aggarwal,^{1,*} Alberto Rolandi,^{2,3,*} Yikai Yang,¹ Joseph Hickie,⁴ Daniel Jirovec,⁵ Andrea Ballabio,⁶ Daniel Chrustina,⁶ Giovanni Isella,⁶ Mark T. Mitchison,^{7,8} Martí Perarnau-Llobet,^{9,2} and Natalia Ares¹

¹Department of Engineering Science, University of Oxford, Parks Road, Oxford OX1 3PJ, United Kingdom

²Département de Physique Appliquée, Université de Genève, 1211 Genève, Switzerland

³Atominstitut, TU Wien, 1020 Vienna, Austria

⁴Department of Materials, University of Oxford, Parks Road, Oxford OX1 3PH, United Kingdom

⁵Institute of Science and Technology Austria, Am Campus 1, 3400 Klosterneuburg, Austria

⁶L-NESS, Physics Department, Politecnico di Milano, via Anzani 42, 22100, Como, Italy

⁷School of Physics, Trinity College Dublin, College Green, Dublin 2, D02 K8N4, Ireland

⁸Trinity Quantum Alliance, Unit 16, Trinity Technology and Enterprise Centre, Pearse Street, Dublin 2, D02 YN67, Ireland

⁹Física Teòrica: Informació i Fenòmens Quàntics, Departament de Física, Universitat Autònoma de Barcelona, 08193 Bellaterra (Barcelona), Spain

The conversion of thermal energy into work is usually more efficient in the slow-driving regime, where the power output is vanishingly small. Efficient work extraction for fast driving protocols remains an outstanding challenge at the nanoscale, where fluctuations play a significant role. In this Letter, we use a quantum-dot Szilard engine to extract work from thermal fluctuations with maximum efficiency over two decades of driving speed. We design and implement a family of optimised protocols ranging from the slow- to the fast-driving regime, and measure the engine's efficiency as well as the mean and variance of its power output in each case. These optimised protocols exhibit significant improvements in power and efficiency compared to the naive approach. Our results also show that, when optimising for efficiency, boosting the power output of a Szilard engine inevitably comes at the cost of increased power fluctuations.

I. Introduction

Converting thermal energy into work is the central problem of thermodynamics. Efficient work extraction typically requires reversible, quasi-static operations and thus vanishing power output on average [1]. This trade-off between efficiency and power also extends to the fluctuations, which must diverge to achieve finite power at maximum (Carnot) efficiency [2, 3]. The need for efficient work extraction protocols for systems driven in a finite time, and hence under far-from-equilibrium conditions, thus naturally arises.

Information engines, such as the paradigmatic Szilard engine [4], provide an ideal setting to address this problem. Information obtained through a measurement can be exploited to entirely convert thermal energy to work, in principle [5–7]. In an information engine, therefore, any loss of efficiency results from the non-equilibrium nature of the driving protocol. By contrast, in conventional heat-driven engines, efficiency is limited both by non-equilibrium effects and by the need to dump some energy into a cold bath to ensure consistency with the second law of thermodynamics. Inferring the efficiency of a thermal engine, therefore, requires independent measurements of heat and work, which remains a challenging task at the nanoscale despite recent progress [8–11].

While information-to-work conversion has a long history, dating back to seminal ideas of Maxwell, Szilard and Landauer [4, 12, 13], its experimental implementation is more recent and has been driven by devel-

opments in the fields of stochastic and quantum thermodynamics [14, 15]. Pioneering experiments have realised a Szilard engine [16] and the erasure of information close to the Landauer limit [17] on single colloidal particles. These were followed by several experiments exploring the link between information and thermodynamics in Brownian colloidal particles [18–20] and a variety of other platforms such as quantum dots [21–23], ultracold atoms [24], quantum memories [25] and superconducting circuits [26, 27]. However, while optimal extraction of work from information has been demonstrated in the slow-driving regime [23], the more challenging case of arbitrary driving speeds is yet to be addressed.

Here we address this challenge by implementing optimal work extraction in a quantum-dot Szilard engine operated over two orders of magnitude in driving speed. The optimal protocol is found using a similar technique to that of the theoretical results of Ref. [28], which interpolates between the two-jump protocols for fast driving [29, 30] and the geodesic protocols of Ref. [31] at slow driving. We also characterise work fluctuations, which play a dominant role at these scales [32]. We observe that, whereas in the high efficiency regime work fluctuations disappear due to the fluctuation-dissipation relation, higher power comes inevitably with higher fluctuations.

II. Experiment

Our device is shown in Fig. 1(a). It consists of a quantum dot defined in a strained germanium quantum well. An information bit is encoded in the occupancy of the right dot in the bottom array (QD1). This quantum dot QD1 is defined by applying voltages V_{G1} and V_{G3} . The quantum dot's electrochemical potential ε is controlled using

* These authors have contributed equally to this work.

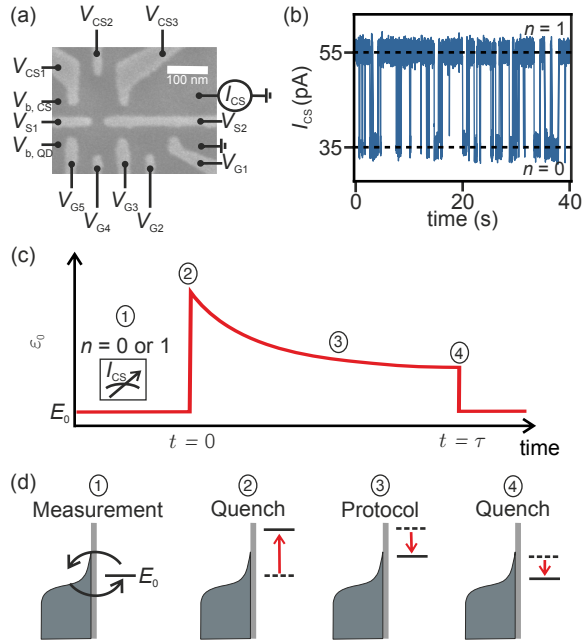


FIG. 1. (a) Scanning electron microscope image of the device. The quantum dot encoding an information bit is controlled using gate voltages V_{G1-G5} . The charge sensor quantum dot is defined using gate voltages $V_{CS1-CS3}$. (b) A time trace of the current I_{CS} through the charge sensor showing the stochastic tunneling of a particle in the information quantum dot. (c) In the first step, the quantum dot is initialised at 50% – 50% and pulsed to a known state. (d) It is reset to the initial state and in process gaining energy, realising a Szilard engine.

the plunger gate voltage V_{G2} . The left dot in the array is tuned in Coulomb blockage, limiting the tunnelling of QD1 to the right reservoir. Another quantum dot in the top array, defined using gates $V_{CS1-CS3}$, serves as a probe for the occupancy n of QD1. The occupancy n is monitored by measuring the current I_{CS} flowing through the charge sensor dot as shown in Fig. 1(b).

The experiment is performed in a regime where $n \in \{0, 1\}$ i.e., when QD1 has an effective occupation of 0 or 1. The tunnelling rates in and out of QD1 are characterised by $\gamma_{in} = \Gamma_{in}f(\varepsilon)$ and $\gamma_{out} = \Gamma_{out}(1-f(\varepsilon))$, where $\Gamma_{in} = 3.5$ Hz and $\Gamma_{out} = 7.0$ Hz, where $f(x) = (1+e^{\beta x})^{-1}$ is the Fermi function and $\beta = (k_B T)^{-1}$ is the inverse of the system's temperature ($T = 180$ mK). We note that $\Gamma_{out} \approx 2\Gamma_{in}$ indicating the spin degeneracy of the system. The characterisation of the tunnelling rates, electron temperature and lever arm is presented in App. B.

In this Letter, we operate this device as a Szilard engine, the details of which are described in the next section. From an operational perspective this requires us to let the quantum dot system thermalise with the reservoir while keeping its energy at $E_0 = k_B T \ln 2$ which corresponds to a 50% – 50% occupation, where T is the electron temperature. Then the charge sensor measures the instantaneous charge state, and the gate voltage V_{G2} is modified to realise the optimal protocol as shown in

Fig. 1(c,d).

III. Szilard Engine and Optimisation

In this section we will present how the setup can be used as a Szilard engine and then proceed to optimise it. The quantum dot can be effectively described as a two-level system where the state $|0\rangle$ corresponds to the dot being empty and the state $|1\rangle$ corresponds to the dot being occupied. The Hamiltonian of the system would then be $\hat{H}(t) = \varepsilon(t)\hat{a}^\dagger\hat{a}$ where $\varepsilon(t)$ is the energy gap between the energy levels – which can be controlled by the gate voltage V_{G2} – and $\hat{a} = |0\rangle\langle 1|$. We can take the environment to be a thermal bath at inverse temperature β . Therefore, by denoting with $p(t)$ the probability of being in the excited state, the rate equation of the system becomes

$$\dot{p} = \gamma[2f(\varepsilon) - (1 + f(\varepsilon))p], \quad (1)$$

where $\gamma = \Gamma_{in}$. The main goal when designing a thermal engine is to find the appropriate function $\varepsilon(t)$ so that (on average) one can extract thermodynamic work in some finite time τ :

$$\mathcal{W}[\varepsilon(t)] - \int_0^\tau dt \text{Tr}[\hat{\rho} \frac{d}{dt} \hat{H}(t)] = - \int_0^\tau dt p(t)\dot{\varepsilon}(t), \quad (2)$$

where we chose the sign convention so that \mathcal{W} is positive when energy is gained from the system.

As opposed to typical heat engines – which use a hot and a cold bath, a Szilard engine makes use of a single thermal bath and measurements on the working substance. From a thermodynamic perspective, the resource provided by the measurement is similar to that of a zero-temperature thermal bath [33, 34]. The steps in the cycle of a Szilard quantum dot engine can be broken down as follows (cf. Fig. 1(c,d)): 0) The energy gap starts at E_0 so that $p = 1/2$ and the system is always in contact with the bath. 1) Measure the occupation of the dot with the charge sensor. 2) If the outcome of the measurement at step 1 is that the dot is in the state $|0\rangle$ ($n = 0$), quickly increase ε to a large value; if instead the outcome is $|1\rangle$ ($n = 1$), quickly decrease ε to a large negative value. 3) The energy gap is brought back towards E_0 in some finite time τ . For the cycle corresponding to a measurement of the state $|0\rangle$, the protocol is designed to use the information of the measurement so that step 2 is free and we are always in a position of gaining energy during step 3 since the probability of a jump occurring is non-zero. However, by Landauer's principle, at the measurement in step 1 there is an implicit cost of $k_B T \ln 2$ that will be paid when the memory storing the result is erased.

Here we turn towards the optimisation of the protocol: for a given total cycle time τ , what is the function $\varepsilon(t)$ that maximises the functional $\mathcal{W}[\varepsilon(t)]$? In general, this is a highly non-trivial problem which requires approximations to be solved, e.g. slow or fast driving limits for analytical results or by making use of numerical techniques such as reinforcement learning [30, 35–37]. However, the

dynamics of the system at hand are simple enough to obtain a general analytical solution for $\varepsilon(t)$ and $p(t)$ without any further approximation, using an approach similar to [28]. Here we will focus on finding and characterizing the optimal protocol $\varepsilon_0(t)$ in the case that we measure $|0\rangle$ in step 1, as the derivation for the case in which we measure $|1\rangle$ is completely analogous. Since we have to perform cycles, the symmetry of the problem imposes the boundary conditions $\varepsilon(0) = \varepsilon(\tau) = E_0$. We start by integrating by parts the definition of work gain

$$\mathcal{W}[\varepsilon(t)] = p(\tau)E_0 + \int_0^\tau dt \dot{p}(t)\varepsilon(t) , \quad (3)$$

where we used the fact that $p(0) = 0$. Therefore, for the bulk of the protocol, maximising the work gain is equivalent to maximising the heat flux $\mathcal{Q}[\varepsilon(t)] = \int_0^\tau dt \dot{p}(t)\varepsilon(t)$. By using the fact that the dynamics are defined by eq. (1), we can write $\varepsilon(t)$ as a function of $p(t)$ and $\dot{p}(t)$:

$$\beta\varepsilon(t) = \ln \left[\frac{2-p(t)}{p(t)+\dot{p}(t)} - 1 \right] , \quad (4)$$

where we are using time units such that $\gamma = 1$. This allows us to write the work gain as a functional of $p(t)$ and $\dot{p}(t)$:

$$\mathcal{W}[p(t), \dot{p}(t)] = p(\tau)E_0 + k_B T \int_0^\tau dt \mathcal{L}[p(t), \dot{p}(t), t] , \quad (5)$$

where $\mathcal{L}[p, \dot{p}, t] = \dot{p} \ln \left[\frac{2-p}{p+\dot{p}} - 1 \right]$. Since $\partial\mathcal{L}/\partial t = 0$, the Euler-Lagrange equation to obtain the function $p(t)$ that extremises work can be written as

$$\dot{p}^2 \frac{2-p}{(p+\dot{p})(2-2p-\dot{p})} = K , \quad (6)$$

where $K := \mathcal{L} - \dot{p} \frac{\partial\mathcal{L}}{\partial\dot{p}}$ is a constant for the solution of the Euler-Lagrange equation. We can solve for \dot{p} to obtain

$$\dot{p} = \frac{1}{2} \frac{K(2-3p) + \sqrt{\Delta}}{2-p+K} , \quad (7)$$

where $\Delta = K^2(2-p)^2 + 8Kp(1-p)(2-p)$. We assumed $\dot{p} > 0$ since we are in the scenario where we measured the state to be $|0\rangle$ at $t = 0$, and therefore $p(0) = 0$. We can solve this differential equation to find the solution

$$t = \int_{p(0)}^{p(t)} dp \frac{4-2p}{K(2-3p) + \sqrt{\Delta}} . \quad (8)$$

We therefore have an implicit formula (via function inversion) for the optimal probability trajectory as a function of time and the integration constant: $p(t) = F_K^{-1}(t)$, where we define F_K to be the solution of the integral in eq. (8) for $p(0) = 0$.

Furthermore, by combining eq. (7) and eq. (5) we can obtain a formula for the maximal amount of extracted

work as a function of the boundary conditions and the integration constant K :

$$\max_{\varepsilon(t)} \mathcal{W}[\varepsilon(t)] = p(\tau)E_0 + k_B T G_K(p(\tau)) , \quad (9)$$

with

$$G_K(P) := \int_0^P dp \ln \left[\frac{2(2-p)(2-p+K)}{(2-p)(K+2p) + \sqrt{\Delta}} - 1 \right] . \quad (10)$$

The measurement at step 1 sets the boundary condition $p(0) = 0$. Since at the start of the next cycle another measurement will be performed, we do not need to impose a boundary condition at $p(\tau)$. Therefore by replacing $p(\tau)$ with $F_K^{-1}(\tau)$ in eq. (9) and maximising with respect to K we can find the optimal integration constant κ_τ (for a given protocol time τ) which defines the optimal protocol:

$$\beta\varepsilon_0(t) = \ln \left[\frac{2(2-p)(2-p+K)}{(2-p)(K+2p) + \sqrt{\Delta}} - 1 \right] \Big|_{p=F_{\kappa_\tau}^{-1}(t)} . \quad (11)$$

Since the optimal integration constant is defined by

$$\kappa_\tau := \arg \min_K F_K^{-1}(\tau)E_0 + G(F_K^{-1}(\tau)) , \quad (12)$$

we turned the functional minimisation problem in eq. (5) into a regular minimisation problem, which is much simpler to handle numerically. It can be noted from eq. (11) that $\varepsilon(0) > E_0$ by taking $p(0) = 0$. Furthermore, we can also confirm numerically that $\varepsilon(\tau) > E_0$. This allows us to conclude that the optimal protocols features jumps at the start and the end of the protocol. In Fig. 2(a) we showcase these optimal protocols for a range of values of $\gamma\tau$ from the slow-driving regime to the fast-driving regime. One can note the qualitative difference of these optimal protocols at the opposite ends of the spectrum of driving speeds. On the one hand, in the fast driving regime, optimal protocols feature very little continuous control and consist of mainly one jump at the start and one at the end – these protocols are also known as “bang-bang protocols” [30]. On the other hand, in the slow driving regime, the optimal protocols do not feature a jump at the end and consist of a smooth and continuous driving of the system’s energy, which matches with previous results in the literature [38].

IV. Results and discussion

For the engine cycle to be truly closed, the information obtained from the measurement in step 1 will eventually have to be erased, thus dissipating at least $k_B T \ln 2$ of heat into the environment because of Landauer’s principle. This gives us a simple formula for the efficiency of this engine

$$\eta = \frac{\mathcal{W}}{k_B T \ln 2} . \quad (13)$$

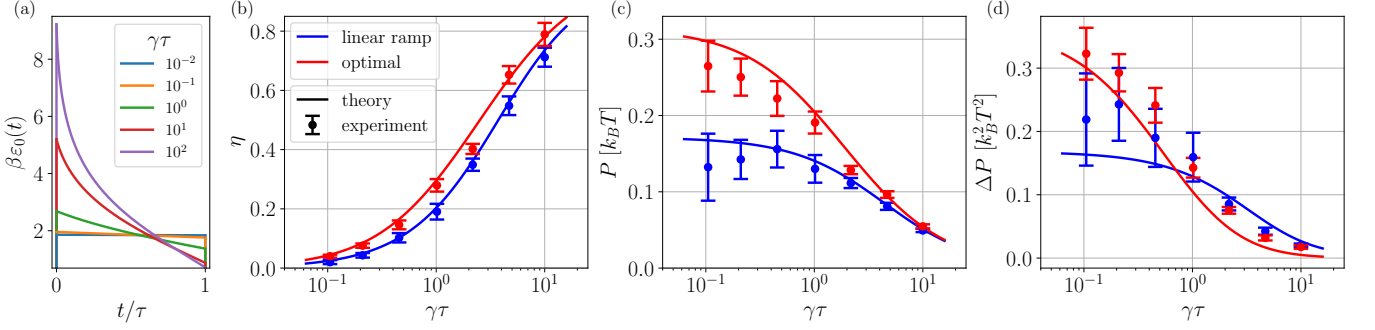


FIG. 2. (a) Optimal protocol for different values of $\gamma\tau$. (b, c, d) Comparison of predicted and measured efficiency $\eta = \beta\mathcal{W}/\ln 2$ (b), power $P = \mathcal{W}/\tau$ (c), and power fluctuations $\Delta P = \text{Var}(P)$ (d) for implementations of the optimal protocol eq.(11) (red) and a linear ramp $\varepsilon(t) = E_0 + 5k_B T(\tau - t)/\tau$ (blue) at different values of $\gamma\tau$ that range from the fast-driving regime to the slow-driving regime.

The efficiency of the information engine reaches its maximum $\eta_C = 1$ in the static limit, which corresponds to the Carnot efficiency that one obtains when setting the temperature of the cold bath to zero. This is simply one of many examples of the link between perfect measurements and zero-temperature baths [33, 34].

It is interesting to note that this expression for efficiency implies that, for a given cycle length τ , the optimisation of power and efficiency coincide. It is therefore sufficient to maximise the work gained to optimise both the power and efficiency. In Fig. 2(b, c) we show as red solid lines the maximal efficiency and maximum power that can be achieved for a given value of $\gamma\tau$, and as dots with error-bars the measured work extracted from in the experimental realisation. The error is computed as the uncertainty statistical uncertainty of the measured work (cf. App. D). Since the dot's occupation is measured continuously throughout the implementation of the protocol, we used the dot's occupation data to compute the work cost of a single round of the experiment, with multiple repetitions – in the thousands for the faster protocols and at least 200 for the slower ones.

One can further optimise the engine for either power or efficiency by considering also the cycle duration τ . Indeed, we can see that in the slow driving regime the efficiency tends to the Carnot efficiency and the power vanishes. Conversely, in the fast driving regime the power is reaching a maximum and the efficiency is vanishing.

We also compare the obtained results and measurements to the power and efficiency of a “naive protocol”: a linear ramp from $E_0 + 5k_B T$ to E_0 over the whole cycle length τ . We can see that the difference is not very significant in terms of efficiency. However, for power, the optimal protocol has significant gains in the fast driving regime. In Fig. 2(d) we computed and measured the power fluctuations of these protocols

$$\Delta P := \frac{2}{\tau} \int_0^\tau dt \int_0^t dt' \dot{\varepsilon}(t) \dot{\varepsilon}(t') p(t') (q(t|t') - p(t)) , \quad (14)$$

where $q(t|t')$ is the probability of the dot being in the state $|1\rangle$ at time t given that it was in state $|1\rangle$ at time $t' < t$.

The wide range of driving speeds that we had access to with the experiment allows us to appreciate how the trade-off between power optimisation and fluctuations optimisation changes depending on the driving speed. The protocols that we implemented optimise the work extracted for a given protocol duration. Therefore, for that fixed protocol duration, the power and efficiency of the Szilard engine will be optimal. Whereas the fluctuations are not optimised for, and therefore should not be expected to be optimal. Indeed, in the fast driving regime we can see that the engine has large fluctuations – in addition to the low efficiency. However, in the slow driving regime we can recover the fluctuation-dissipation relation $\frac{\tau\beta}{2} \Delta P = -\mathcal{W} - \Delta F$ [39–41], where $\Delta F = -k_B T \ln 2$ is the difference in free energy between the start and end of the protocol. This relation shows that maximising the extracted work is equivalent to minimising fluctuations in the slow driving regime. We therefore expect our engine to also be optimal for fluctuations in this regime: in Fig. 2(d) we can observe that the measured fluctuations become vanishing as we increase the protocol length.

In general, the level of agreement between experimental results and theoretical predictions is high. However, it is worth noting that there seems to be a mismatch between the measured values of fluctuations and the predicted values. This can be caused by a number of reasons, however, the most significant here is a drift in the calibration of the experiment over time, which introduces a bias in the implemented protocol. Indeed, to accurately measure the fluctuations of work one needs a much larger number of samples compared to the number of runs needed to accurately measure the average of the work extracted. This need for a large number of samples gives an additional disadvantage: the more time is needed to perform the measurements the more apparatus' calibration drift will affect the measurements. This can be seen in Fig. 2(d) for the protocols with $1 < \gamma\tau < 10$, as the repeated implementation of these left more time for the quantum dot's calibration to drift. Indeed, for these protocols we see that the predicted value for fluctuations is in a larger disagreement with the measurement compared to the fast protocols with $0.1 < \gamma\tau < 1$. However, such

a large disagreement is not observed for the predicted power and efficiency, even if they are computed from the same data that experienced the same calibration drift. This mismatch of precision between the predicted values is explained by the fact that the implemented protocols are close to being optimal for power and efficiency, even with the drift. Therefore, for small deviation $\delta\varepsilon$ from the optimal protocol, the power and efficiency will be affected by a factor proportional to $\delta\varepsilon^2$, since the optimal protocol extremizes the power and efficiency. Conversely, the fluctuations are not optimised by the protocols being implemented, meaning the deviations from the protocol will affect them by a factor proportional to $\delta\varepsilon$ instead of $\delta\varepsilon^2$. This corresponds perfectly with the observations in Fig. 2, where the deviations from the theoretical values are larger for the fluctuations than for the power and efficiency. In App. C we explore this further by analysing quantitatively how much the power and fluctuations change for a constant shift from the optimal protocol $\varepsilon(t) \rightarrow \varepsilon(t) + \Delta$, finding very good agreement with the qualitative description provided above.

Furthermore, it is worth noting that this difference in scaling to small variations from the optimal protocol can be potentially be exploited to sacrifice a small amount of power and efficiency to obtain a comparatively large reduction in fluctuations.

V. Conclusion

We implemented and optimised a Szilard engine, where information gained through measurement allows for the extraction of work in the presence of a single heat bath. This represents a minimal model to explore the extraction of work from thermal fluctuations. The experimental setup consisted of a quantum dot system in a germanium quantum well, where the occupancy of the dot can be manipulated and monitored. Using this system, we successfully implemented an optimised finite-time Szilard engine over two decades of driving speed ($10^{-1} \leq \gamma\tau \leq 10^1$), spanning both fast- and slow-driving regimes.

Our optimisation procedure maximises the extracted energy for a given, arbitrary, cycle length. In our system, this allows for the simultaneous optimisation of power and efficiency. These optimal protocols showed significant improvements in power and efficiency over a naive linear ramp protocol at all driving speeds, in particular in the fast driving regime. Additionally, we examined the

work fluctuations generated by these optimal protocols, and observed that higher power inevitably comes with higher fluctuations. However, we also observed that, by slightly deviating from the power-optimal protocol, one can accept a small reduction in power in exchange for a large reduction in fluctuations thanks to the fact that we are operating close to optimum for power.

The experimental results corroborated the theoretical predictions, showing a high degree in precision of the (indirect) measurement of extracted work. However, for the fluctuations, it seems that the measured values are in larger disagreement with the theory than the corresponding measurements of work (more than 1σ away for most values). This bias can be explained by the fact that the calibration of the experiment drifts over time. Despite this, the overall agreement between theory and experiment for the extracted work shows the feasibility of these optimal protocols in information engines and opens new avenues of implementation on this type of platforms [42]. For example, to study the thermodynamics of collective phenomena [37], or to evaluate work fluctuations and their optimization [30, 43, 44].

Acknowledgments

We thank Georgios Katsaros for providing the device for this experiment. K.A. and N.A. acknowledge the support provided by funding from the Engineering and Physical Sciences Research Council IAA (Grant number EP/X525777/1). N.A. acknowledges support from the European Research Council (grant agreement 948932) and the Royal Society (URF-R1-191150). A.R. is supported by the Swiss National Science Foundation through a Postdoc.Mobility (Grant No. P500PT 225461). M.T.M. is supported by a Royal Society-SFI University Research Fellowship (URF\R1\221571). M.P.-L. acknowledges support from the Spanish Agencia Estatal de Investigacion through the grant “Ramón y Cajal RYC2022-036958-I”. This project is co-funded by the European Union and UK Research & Innovation (Quantum Flagship project ASPECTS, Grant Agreement No. 101080167). Views and opinions expressed are however those of the authors only and do not necessarily reflect those of the European Union, Research Executive Agency or UK Research & Innovation. Neither the European Union nor UK Research & Innovation can be held responsible for them.

[1] N. Shiraishi, K. Saito, and H. Tasaki, *Phys. Rev. Lett.* **117**, 190601 (2016).

[2] M. Campisi and R. Fazio, *Nature Communications* **7**, 11895 (2016).

[3] P. Pietzonka and U. Seifert, *Phys. Rev. Lett.* **120**, 190602 (2018).

[4] L. Szilard, *Behavioral Science* **9**, 301 (1964).

[5] R. Landauer, *Physics Today* **44**, 23–29 (1991).

[6] J. M. R. Parrondo, J. M. Horowitz, and T. Sagawa, *Nature Physics* **11**, 131–139 (2015).

[7] J. d. Buisson, D. A. Sivak, and J. Bechhoefer, “Performance limits of information engines,” (2024).

[8] M. Josefsson, A. Svilans, A. M. Burke, E. A. Hoffmann, S. Fahlvik, C. Thelander, M. Leijnse, and H. Linke, *Nature Nanotechnology* **13**, 920 (2018).

[9] B. Karimi, F. Brange, P. Samuelsson, and J. P. Pekola, *Nature Communications* **11**, 367 (2020).

[10] D. Majidi, M. Josefsson, M. Kumar, M. Leijnse,

L. Samuelson, H. Courtois, C. B. Winkelmann, and V. F. Maisi, *Nano Letters* **22**, 630 (2022).

[11] D. Majidi, J. P. Bergfield, V. Maisi, J. Höfer, H. Courtois, and C. B. Winkelmann, *Applied Physics Letters* **124**, 140504 (2024).

[12] J. C. Maxwell, *Theory of Heat* (Cambridge University Press, 2011).

[13] R. Landauer, *IBM journal of research and development* **5**, 183 (1961).

[14] S. Ciliberto, *Phys. Rev. X* **7**, 021051 (2017).

[15] N. M. Myers, O. Abah, and S. Deffner, *AVS Quantum Science* **4** (2022), 10.1116/5.00083192.

[16] S. Toyabe, T. Sagawa, M. Ueda, E. Muneyuki, and M. Sano, *Nature Physics* **6**, 988–992 (2010).

[17] A. Bérut, A. Arakelyan, A. Petrosyan, S. Ciliberto, R. Dillenschneider, and E. Lutz, *Nature* **483**, 187–189 (2012).

[18] Y. Jun, M. c. v. Gavrilov, and J. Bechhoefer, *Phys. Rev. Lett.* **113**, 190601 (2014).

[19] G. Paneru, D. Y. Lee, T. Tlusty, and H. K. Pak, *Phys. Rev. Lett.* **120**, 020601 (2018).

[20] T. Admon, S. Rahav, and Y. Roichman, *Phys. Rev. Lett.* **121**, 180601 (2018).

[21] J. V. Koski, V. F. Maisi, J. P. Pekola, and D. V. Averin, *PNAS* **111**, 13786 (2014).

[22] D. Barker, M. Scandi, S. Lehmann, C. Thelander, K. A. Dick, M. Perarnau-Llobet, and V. F. Maisi, *Phys. Rev. Lett.* **128**, 040602 (2022).

[23] M. Scandi, D. Barker, S. Lehmann, K. A. Dick, V. F. Maisi, and M. Perarnau-Llobet, *Phys. Rev. Lett.* **129**, 270601 (2022).

[24] A. Kumar, T.-Y. Wu, F. Giraldo, and D. S. Weiss, *Nature* **561**, 83–87 (2018).

[25] P. A. Camati, J. P. Peterson, T. B. Batalhão, K. Micaudei, A. M. Souza, R. S. Sarthour, I. S. Oliveira, and R. M. Serra, *Physical Review Letters* **117** (2016), 10.1103/physrevlett.117.240502.

[26] N. Cottet, S. Jezouin, L. Bretheau, P. Campagne-Ibarcq, Q. Ficheux, J. Anders, A. Auffèves, R. Azouit, P. Rouchon, and B. Huard, *Proceedings of the National Academy of Sciences* **114**, 7561–7564 (2017).

[27] Y. Masuyama, K. Funo, Y. Murashita, A. Noguchi, S. Kono, Y. Tabuchi, R. Yamazaki, M. Ueda, and Y. Nakamura, *Nature Communications* **9** (2018), 10.1038/s41467-018-03686-y.

[28] M. Esposito, R. Kawai, K. Lindenberg, and C. V. den Broeck, *EPL (Europhysics Letters)* **89**, 20003 (2010).

[29] S. Blaber, M. D. Louwerve, and D. A. Sivak, *Phys. Rev. E* **104**, L022101 (2021).

[30] A. Rolandi, M. Perarnau-Llobet, and H. J. D. Miller, *New Journal of Physics* **25**, 073005 (2023).

[31] M. Scandi and M. Perarnau-Llobet, *Quantum* **3**, 197 (2019).

[32] C. Jarzynski, *Annual Review of Condensed Matter Physics* **2**, 329 (2011).

[33] Y. Guryanova, N. Friis, and M. Huber, *Quantum* **4**, 222 (2020).

[34] P. Taranto, F. Bakhshinezhad, A. Bluhm, R. Silva, N. Friis, M. P. Lock, G. Vitagliano, F. C. Binder, T. Debarba, E. Schwarzhans, F. Clivaz, and M. Huber, *PRX Quantum* **4** (2023), 10.1103/prxquantum.4.010332.

[35] A. Rolandi and M. Perarnau-Llobet, *Quantum* **7**, 1161 (2023).

[36] P. A. Erdman, A. Rolandi, P. Abiuso, M. Perarnau-Llobet, and F. Noé, *Phys. Rev. Res.* **5**, L022017 (2023).

[37] A. Rolandi, P. Abiuso, and M. Perarnau-Llobet, *Physical Review Letters* **131** (2023), 10.1103/physrevlett.131.210401.

[38] P. Abiuso and M. Perarnau-Llobet, *Phys. Rev. Lett.* **124**, 110606 (2020).

[39] J. Weber, *Physical Review* **101**, 1620–1626 (1956).

[40] R. Kubo, *Reports on Progress in Physics* **29**, 255–284 (1966).

[41] H. J. D. Miller, M. Scandi, J. Anders, and M. Perarnau-Llobet, *Phys. Rev. Lett.* **123**, 230603 (2019).

[42] J. Dunlop, F. Cerisola, J. Monsel, S. Sevitz, J. Tabanera-Bravo, J. Dexter, F. Fedele, N. Ares, and J. Anders, “Extra cost of erasure due to quantum lifetime broadening,” (2024).

[43] T. Denzler, J. F. G. Santos, E. Lutz, and R. M. Serra, *Quantum Science and Technology* **9**, 045017 (2024).

[44] T. Denzler and E. Lutz, *Phys. Rev. Res.* **3**, L032041 (2021).

[45] D. Jirovec, A. Hofmann, A. Ballabio, P. M. Mutter, G. Tavani, M. Botifoll, A. Crippa, J. Kukucka, O. Sagi, F. Martins, J. Saez-Mollejo, I. Prieto, M. Borovkov, J. Arbiol, D. Chrastina, G. Isella, and G. Katsaros, *Nature Materials* **20**, 1106–1112 (2021).

[46] A. Hofmann, V. F. Maisi, C. Rössler, J. Basset, T. Krähenmann, P. Märki, T. Ihn, K. Ensslin, C. Reichl, and W. Wegscheider, *Phys. Rev. B* **93**, 035425 (2016).

A. Device fabrication

The devices were processed in the Institute of Science and Technology Austria Nanofabrication facility. A 6x6 mm² chip comprising of Ge quantum well sandwiched between Si_{0.3}Ge_{0.7} is cleaned before further processing. Further details about the quantum well growth can be found in Ref. [45]. First, ohmic contacts are patterned in a 100 keV electron beam lithography system. Subsequently, a few nanometers of native oxide is milled by argon bombardment which is followed by deposition of 60 nm Pt layer. A 20 nm thick layer of aluminium oxide is deposited at 300°C in an atomic layer deposition step, followed by gates consisting of 3 nm Ti and 27 nm Pd.

B. Characterisation of the tunnel rates and lever arm

The measurements were performed in a dilution refrigerator at a base temperature of 150 mK. The charge sensor and the double quantum dot are isolated by creating an electrostatic barrier using splitter gate voltages V_{S1-S2} . The double quantum dot in the bottom array is tuned by using the gates voltages V_{G2} and V_{G4} . The tunneling between Fermi reservoirs and double quantum dot is controlled using gate voltages V_{G1} and V_{G5} . The inter-dot tunneling is

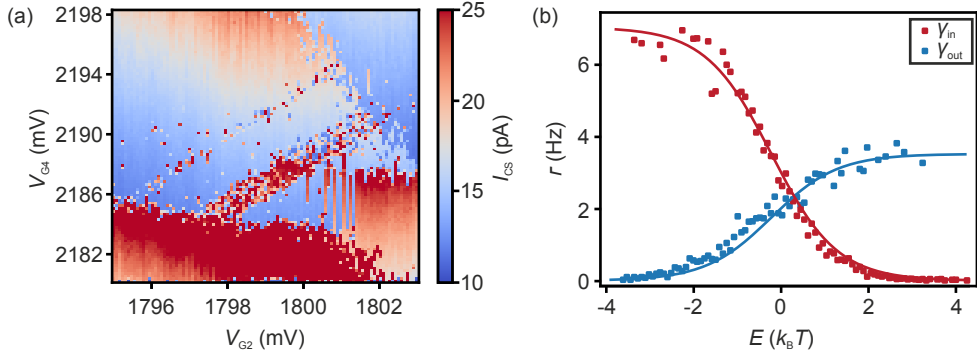


FIG. 3. (a) A set of bias triangles measured by varying V_{G2} and V_{G4} and recording the current I_{CS} through the charge sensor at a bias voltage $V_{b, QD} = 0.32$ mV. (b) Tunneling rates γ_{in} and γ_{out} of QD1.

set by the gate voltage V_{G3} . Similarly, the charge sensor is tuned by a combination of gate voltages $V_{CS1-CS3}$. We first measure a set of bias triangles, as shown in Fig. 3(a), at a fixed bias $V_{b, QD} = 0.32$ mV. We extract a lever arm $\alpha = \frac{V_{b, QD}}{\Delta V_{G2}} = 0.041 \pm 0.002$. Time traces across the transition from $n = 0$ to $n = 1$ were recorded. Tunnel rates and electron temperature were extracted in Fig. 3(b) using the functions: $\gamma_{in} = \Gamma_{in}f(E)$ and $\gamma_{out} = \Gamma_{out}(1 - f(E))$, where $f(E) = (1 + e^{E/k_B T})^{-1}$, which describe the tunneling in and out rates of the quantum dot [46]. We obtain an electron temperature of $T = 180$ mK from these fits.

C. Calibration drift

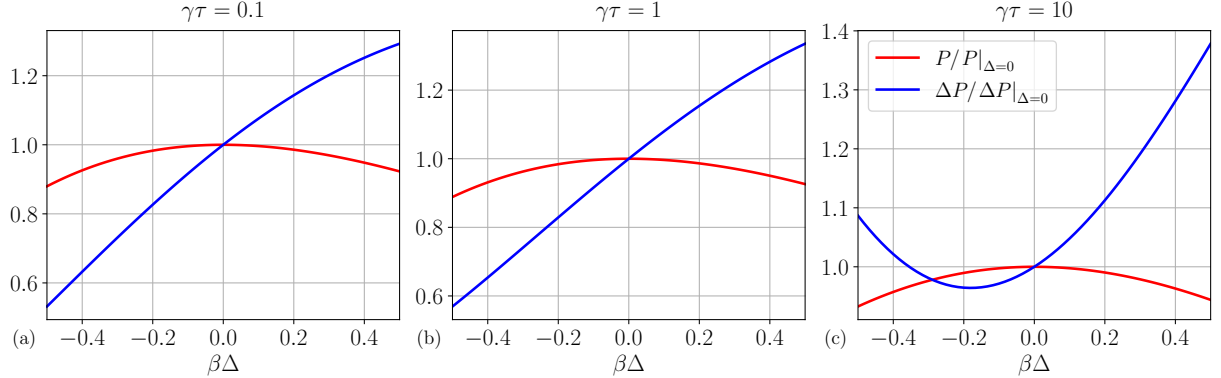


FIG. 4. Relative change of power and fluctuations for a constant shift from the optimal protocol $\varepsilon(t) \rightarrow \varepsilon(t) + \Delta$ for all the regimes of driving speeds: (a) $\gamma\tau = 0.1$, (b) $\gamma\tau = 1$, (c) $\gamma\tau = 10$.

Since the calibration drift takes much longer than the duration of a single cycle (even in the slow driving regime) we can assume that within a cycle it corresponds to a constant shift of the energy $\varepsilon \rightarrow \varepsilon + \Delta$. In Fig. 4 we show how this shift affects the power and fluctuations relative to their value in absence of the shift. As expected, since the power is optimal for $\Delta = 0$, we see that for small shifts it deviates from its optimal value as $\mathcal{O}(\Delta^2)$. Conversely, it is clear that this is not the case for ΔP since the protocols do not optimise the fluctuations. Therefore its deviations scale as $\mathcal{O}(\Delta)$. This makes the fluctuations more sensitive than the power to this shift caused by the calibration drift.

D. Measurement statistics

In this section we present how to compute the estimators – and their variance – for expected work and work fluctuations that were used for the plotted values and error bars in Fig. 2. For N i.i.d statistical samples $\{W_i\}_{i=1}^N$ of a random variable \mathcal{W} . We estimate the expected value of \mathcal{W} with the mean:

$$E(\{W_i\}_{i=1}^N) := \frac{1}{N} \sum_{i=1}^N W_i. \quad (D1)$$

It is straightforward to compute the expected value and variance of this estimator:

$$\langle E(\{W_i\}_{i=1}^N) \rangle = \langle \mathcal{W} \rangle , \quad (\text{D2})$$

$$\text{Var}(E(\{W_i\}_{i=1}^N)) = \frac{\text{Var}(\mathcal{W})}{N} . \quad (\text{D3})$$

Therefore, with N samples of work gain $\{W_i\}_{i=1}^N$, we compute the expected work with the estimator E and use the square root of its variance for its error in the plots. To compute the variance from the sample, we use the following estimator

$$V(\{W_i\}_{i=1}^N) = \frac{1}{N-1} \sum_{i=1}^N (W_i - E(\{W_i\}_{i=1}^N))^2 , \quad (\text{D4})$$

which we can use also to estimate the fluctuations of the work gain. The expected value and variance of this estimator give

$$\langle V(\{W_i\}_{i=1}^N) \rangle = \text{Var}(\mathcal{W}) , \quad (\text{D5})$$

$$\text{Var}(V(\{W_i\}_{i=1}^N)) = \langle \mathcal{W}^4 \rangle \frac{N(N-4)+1}{N(N-1)^2} - \frac{4\langle \mathcal{W}^3 \rangle \langle \mathcal{W} \rangle}{N} - \frac{\text{Var}(\mathcal{W})^2}{N-1} + \frac{3\langle \mathcal{W}^2 \rangle^2}{N} , \quad (\text{D6})$$

where we can use the maximum likelihood estimators for the 2nd, 3rd and 4th moments – m_2 , m_3 and m_4 respectively – to compute the error of the estimator of the work fluctuations from the statistical samples. These maximum likelihood estimators are given by

$$m_j(\{W_i\}_{i=1}^N) := \frac{1}{N} \sum_i W_i^j , \quad (\text{D7})$$

and satisfy $\langle m_j(\{W_i\}_{i=1}^N) \rangle = \langle \mathcal{W}^j \rangle$.